


Magnetothermopower of Nodal-Line Semimetals

Poulomi Chakraborty^{1,*}, Aaron Hui¹, Grigory Bednik² and Brian Skinner¹

¹*Department of Physics, The Ohio State University, Columbus, Ohio 43202, USA*

²*Department of Physics, University of Nebraska, Omaha, Nebraska 68182, USA*

 (Received 16 March 2024; revised 29 April 2024; accepted 29 May 2024; published 20 June 2024)

The search for materials with large thermopower is of great practical interest. Dirac and Weyl semimetals have recently proven to exhibit superior thermoelectric properties, particularly when subjected to a quantizing magnetic field. Here, we consider whether a similar enhancement arises in nodal-line semimetals, for which the conduction and valence band meet at a line or ring in momentum space. We compute the Seebeck and Nernst coefficients for arbitrary temperature and magnetic field and we find a wealth of different scaling regimes. Most strikingly, when a sufficiently strong magnetic field is applied along the direction of a straight nodal line or in the plane of a nodal ring, the large degeneracy of states leads to a large linear-in- B thermopower that is temperature independent even at low temperatures. Our results suggest that nodal-line semimetals may offer significant opportunity for efficient low-temperature thermoelectrics.

DOI: [10.1103/PRXEnergy.3.023007](https://doi.org/10.1103/PRXEnergy.3.023007)

I. INTRODUCTION

Charge carriers in a solid material generally also carry heat, so that the phenomena of electrical and thermal conduction become mixed. Under steady-state conditions where no current is flowing, a temperature gradient leads to a gradient of carrier concentration and therefore to a measurable voltage difference; this is known as the thermoelectric effect. The strength of the thermoelectric effect is typically characterized by the Seebeck coefficient (thermopower), defined via [1–3]

$$S_{xx} = \frac{(\Delta V)_x}{(\Delta T)_x}, \quad (1)$$

where $(\Delta T)_x$ is the difference in temperature along the x direction and $(\Delta V)_x$ is the voltage difference along the same direction. Identifying or designing materials with large Seebeck coefficient has great utility in practical applications such as thermocouples, thermoelectric coolers, and thermoelectric generators, since the thermoelectric effect allows one to convert waste heat to electric current, or to convert applied electric current to heating or cooling power [4].

In typical conductors, however, the thermoelectric effect is generically weak. For example, in a single-band conductor with a large Fermi surface, the Seebeck coefficient is of order $(k_B/e)(k_B T/E_F)$, where E_F is the Fermi energy and $-e$ is the electron charge [1,5,6]. The quantity $k_B/e \approx 86 \mu\text{V/K}$ represents the natural unit of thermopower. Typical metals, for which $k_B T \ll E_F$, therefore have a greatly suppressed thermopower. On the other hand, materials with low E_F , such as doped semiconductors or insulators, are poor electrical conductors; they can achieve high thermopower but have high electrical resistance, hampering their ability to provide efficient power conversion [3,6,7].

The recently discovered Dirac and Weyl semimetals [8] are potentially very useful for thermoelectric applications because they offer the promise of arbitrarily low Fermi energy combined with robust electrical conductivity. Particularly notable is a strong magnetothermoelectric effect: a series of recent works [9–21] has demonstrated that an applied magnetic field can greatly enhance the thermopower of Dirac and Weyl semimetals while still maintaining metallic-like electrical conduction.

A particularly striking magnetothermoelectric effect has been pointed out in Ref. [13], which has shown that a Dirac or Weyl semimetal can exhibit a nonsaturating linear-in- B growth of the Seebeck coefficient when the magnetic field B is large enough to achieve the extreme quantum limit (EQL), in which all electrons reside in the lowest Landau level. The crux of this effect lies in the way in which a large magnetic field increases the electronic entropy. In the limit where the magnetic field is large enough to produce a large Hall angle (i.e., where electric current flows nearly perpendicular to the electric field), the Seebeck coefficient

*Corresponding author: chakraborty.135@buckeyemail.osu.edu

Published by the American Physical Society under the terms of the [Creative Commons Attribution 4.0 International](https://creativecommons.org/licenses/by/4.0/) license. Further distribution of this work must maintain attribution to the author(s) and the published article's title, journal citation, and DOI.

becomes directly proportional to the electronic entropy [13,14,22–28]:

$$S_{xx} = \frac{n_s}{\rho_e}, \quad (2)$$

where n_s is the entropy density and ρ_e is the charge density of mobile carriers. At low temperatures, the entropy density of an electronic system is directly proportional to the density of states ν near the Fermi level: $n_s \simeq (\pi^2/3)k_B^2 T \nu(E_F)$. Since the degeneracy of a given Landau level, and therefore the value of ν , grows linearly as a function of B , the Seebeck coefficient S_{xx} grows linearly in B when only a single Landau level is occupied. This linear-in- B enhancement of the Seebeck coefficient has been observed experimentally in, e.g., Refs. [15–17,29]. Note, however, that S_{xx} vanishes as $T \rightarrow 0$, such that achieving a large thermopower at low temperature requires a very large magnetic field.

In this paper, we consider whether a similar magnetic field enhancement of thermopower can appear in nodal-line semimetals (NLSs), for which gapless points in the dispersion relation form a one-dimensional (1D) manifold such as a line (illustrated in Fig. 1) or a ring in momentum space [30–34]. We focus on the case in which the nodal line exists at a constant energy and we calculate the longitudinal and transverse thermopower (the Seebeck and Nernst coefficients) as a function of both the temperature and the magnetic field across the entire range of both parameters. We find that the thermopower generally exhibits a strong enhancement with the magnetic field. Most prominently, the thermopower rises linearly with B in the extreme quantum limit, as for Dirac and Weyl semimetals, but for NLSs the flat dispersion along the nodal line enables a huge electronic entropy even at low temperature. Consequently, the Seebeck coefficient in the extreme quantum limit is large, linear in B , and temperature independent at low temperature. This effect may lead to practical low-temperature thermoelectrics. For example, as we show below, in the realistic case of an NLS with electron density $n = 10^{18} \text{ cm}^{-3}$, Fermi velocity $v_F = 10^5 \text{ m/s}$, and a circular nodal line with radius 0.1 \AA^{-1} , increasing the strength of an applied magnetic field from $B = 0$ to $B = 10 \text{ T}$ can increase the thermopower at $T = 10 \text{ K}$ from $S_{xx} \approx 40 \text{ \mu V/K}$ to $S_{xx} \approx 300 \text{ \mu V/K}$. At lower doping, the effect is even more dramatic: an NLS with $n = 10^{17} \text{ cm}^{-3}$ sees its thermopower increase from $S_{xx} \approx 150 \text{ \mu V/K}$ to $S_{xx} \approx 3000 \text{ \mu V/K}$ under the same conditions.

The remainder of this paper is organized as follows. In Sec. II, we explain our mathematical setup and we show how to calculate the Seebeck and Nernst coefficients at arbitrary B and T using two complementary approaches. In Sec. III, we discuss the results for a straight nodal line, considering each regime of B and T . In Sec. IV, we discuss the generalization of our results to the case of a circular

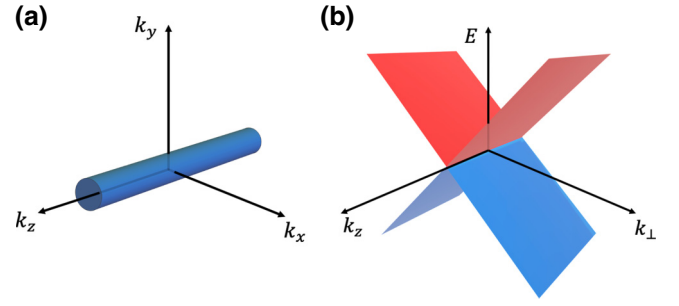


FIG. 1. (a) A schematic of a cylindrical Fermi surface. (b) A plot of the dispersion relation in the k_x - k_y plane, i.e., perpendicular to the direction of the nodal line.

nodal line. We conclude in Sec. V with a summary and a brief discussion of NLS materials and the limitations of our theory.

II. CALCULATIONAL APPROACH

A. Setup and definitions

Our goal in this paper is to compute the thermoelectric tensor \hat{S} as a function of the magnetic field B and temperature T ; the diagonal component of \hat{S} is the Seebeck coefficient (in a particular direction) and the off-diagonal component is the Nernst coefficient. The tensor \hat{S} can be defined by considering the equations that govern the electrical and heat current densities, \mathbf{J}^E and \mathbf{J}^Q :

$$\mathbf{J}^E = \hat{\sigma} \mathbf{E} - \hat{\alpha} \nabla T, \quad (3)$$

$$\mathbf{J}^Q = T \hat{\alpha} \mathbf{E} - \hat{\kappa} \nabla T. \quad (4)$$

Here, \mathbf{E} is the electric field and $\hat{\sigma}$, $\hat{\alpha}$, and $\hat{\kappa}$ are the electrical conductivity, Peltier conductivity, and thermal conductivity tensors, respectively. The appearance of the same coefficient $\hat{\alpha}$ in the “off-diagonal” term of both Eqs. (3) and (4) is a reflection of Onsager reciprocity [1]. The thermoelectric tensor is defined by $\mathbf{E} = \hat{S} \nabla T$ under conditions where the electrical current $\mathbf{J}^E = 0$ [as in Eq. (1)] and therefore

$$\hat{S} = \hat{\sigma}^{-1} \hat{\alpha}. \quad (5)$$

Writing out the Seebeck, S_{xx} , and Nernst, S_{xy} , coefficients explicitly gives

$$S_{xx} = \frac{\alpha_{xx} \sigma_{xx} + \alpha_{xy} \sigma_{xy}}{\sigma_{xx}^2 + \sigma_{xy}^2}, \quad (6)$$

$$S_{xy} = \frac{\alpha_{xy} \sigma_{xx} - \alpha_{xx} \sigma_{xy}}{\sigma_{xx}^2 + \sigma_{xy}^2}. \quad (7)$$

Following Refs. [14,35], we calculate \hat{S} across the full range of B and T by using two complementary approaches.

When many Landau levels are occupied (i.e., when the Landau-level spacing is small compared to the Fermi energy), we can use a semiclassical approach to directly calculate the electrical and Peltier conductivity tensors $\hat{\sigma}$ and $\hat{\alpha}$. In the extreme quantum limit, however, where only a single Landau level is occupied, direct calculation of these tensors becomes difficult. The electron dispersion relation is strongly modified by Landau quantization and the mobility in the field direction becomes strongly different from the mobility in the perpendicular directions. Calculating $\hat{\alpha}$ is particularly subtle, requiring one to invoke Landau-level broadening effects.

Fortunately, at a sufficiently large magnetic field, one can use the generic expression given by Eq. (2), which only requires one to calculate the thermodynamic entropy of the electron system. This formula is valid whenever $\sigma_{xy} \gg \sigma_{xx}$; we refer to this limit as the “dissipationless” limit, since the dissipative conductivity σ_{xx} is negligible. Our two calculational schemes—the semiclassical and dissipationless limits—have an overlapping regime of validity and we show below that both approaches agree quantitatively in the overlap regime.

Throughout this paper, we assume that the charge density of carriers in the nodal band is constant. That is, we take $n_e - n_h = \text{constant}$, where n_e and n_h are the concentration of electron- and hole-type carriers, respectively, in the nodal bands. Both n_e and n_h can in general depend on T and B . This assumption of constant charge density is natural when there are no other trivial bands nearby in energy. In cases in which another band with a large density of states coexists in energy, one can instead have a condition where the chemical potential μ in the nodal band is constant as a function of T and B due to the large trivial band acting as a reservoir. Such pinning of the chemical potential affects the temperature dependence of the thermopower when T is much larger than the Fermi temperature T_F , leading to quantitative but not qualitative changes to the results we discuss below.

B. Semiclassical limit

In the limit of a sufficiently small magnetic field that many Landau levels are occupied, we can ignore Landau quantization effects and calculate the electrical and Peltier conductivity tensors via the usual semiclassical approach [1]:

$$\sigma_{ij} = \int d\epsilon \left(-\frac{\partial f}{\partial \epsilon} \right) \sigma_{ij}(\epsilon), \quad (8)$$

$$\alpha_{ij} = \frac{1}{eT} \int d\epsilon (\epsilon - \mu) \left(-\frac{\partial f}{\partial \epsilon} \right) \sigma_{ij}(\epsilon). \quad (9)$$

Here, $\sigma_{ij}(\epsilon)$ corresponds to the conductivity of carriers at energy ϵ (i.e., to the zero-temperature conductivity when the chemical potential μ is equal to ϵ) and $f(\epsilon) \equiv$

$(\exp(\epsilon - \mu/k_B T) + 1)^{-1}$ is the Fermi-Dirac distribution. Thus, Eq. (8) corresponds to a weighted average of quasiparticle contributions to conductivity in a thermally broadened window around the chemical potential. Similarly, α_{ij} corresponds to a weighted average of quasiparticle contributions to the thermal current under an applied electric field and therefore includes both $(\epsilon - \mu)$ energy and σ_{ij} electrical factors. At low temperatures $T \ll T_F$, a Sommerfeld expansion directly yields the usual Mott formula [1]:

$$\hat{S} = \frac{k_B \pi^2}{e} \frac{1}{3} k_B T \hat{\sigma}(\epsilon)^{-1} \left. \frac{d\hat{\sigma}(\epsilon)}{d\epsilon} \right|_{\epsilon=\mu}. \quad (10)$$

We remark that the Mott formula is generic at low temperature $T \ll T_F$, independent of particular assumptions about $\sigma_{ij}(\epsilon)$. It breaks down only when either $T \gg T_F$, such that one can no longer use a Sommerfeld expansion for the integrals in Eqs. (8) and (9) or when $\hat{\sigma}$ becomes discontinuous as a function of the chemical potential (such as in the regime of strong Landau quantization).

Throughout the main text of this paper, we assume that the chemical potential μ is determined self-consistently from the condition of constant charge density within the nodal-line bands, i.e.,

$$\begin{aligned} n_e - n_h &= \int_0^\infty d\epsilon v(\epsilon) f(\epsilon) - \int_{-\infty}^0 d\epsilon v(\epsilon) (1 - f(\epsilon)) \\ &= \text{const.} \end{aligned} \quad (11)$$

The first term on the right-hand side of this expression represents the number of electrons in the conduction band, while the second term describes the number of holes in the valence band. At low temperatures ($T \ll T_F$), the chemical potential $\mu \simeq E_F$. At high temperatures ($T \gg T_F$), evaluation of Eq. (11) gives a chemical potential $\mu \simeq E_F^2 / (4k_B T \ln 2)$, assuming a low enough temperature that the typical quasiparticle momentum is small compared to the diameter of the nodal line. We discuss in Appendix A how our results are modified if μ is taken to be constant as a function of temperature, as may result from pinning by a trivial electron band that coexists in energy with the nodal-line bands.

In Sec. III, we give special consideration to the case of a straight nodal line, for which the bands are dispersionless in the k_z direction and the dispersion relation is effectively two-dimensional (2D). In this case, only the component $\mathbf{B} \cdot \hat{\mathbf{z}} \equiv B$ of the magnetic field along the z direction is relevant, since electrons have infinite mass along the z direction. In order to calculate the tensors $\hat{\sigma}$ and $\hat{\alpha}$ in this case, we use the relaxation-time approximation with a momentum relaxation time τ . In this case, the

energy-dependent conductivities $\sigma_{ij}(\epsilon)$ are given by

$$\sigma_{xx}(\epsilon) = \frac{v_{2D}(\epsilon)}{2} \frac{e^2 v_F^2 \tau}{1 + \omega_c^2(\epsilon) \tau^2}, \quad (12)$$

$$\sigma_{xy}(\epsilon) = \frac{v_{2D}(\epsilon)}{2} \frac{e^2 v_F^2 \tau}{1 + \omega_c^2(\epsilon) \tau^2} \omega_c(\epsilon) \tau. \quad (13)$$

Here,

$$\omega_c(\epsilon) = \frac{eBv_F^2}{\epsilon} \quad (14)$$

is the energy-dependent cyclotron frequency, in which v_F is the Fermi velocity in the direction perpendicular to the magnetic field and

$$v_{2D}(\epsilon) = \frac{g}{2\pi} \frac{|\epsilon|}{\hbar^2 v_F^2} \quad (15)$$

is the density of states per value of the momentum along the nodal line. The constant g denotes the degeneracy per momentum state (spin \times valley). The full three-dimensional (3D) density of states $\nu(\epsilon)$ is equal to $v_{2D}(\epsilon)$ multiplied by the length of the nodal line in reciprocal space. Note that ω_c has the same sign as the energy ϵ , so that electrons and holes have opposite signs of the cyclotron frequency. For simplicity, we assume throughout this paper that τ is independent of ϵ ; incorporating a power-law energy dependence into τ changes various order-1 numerical coefficients but does not affect the way in which \hat{S} scales with T , B , τ , or E_F [36].

C. Dissipationless limit

In the dissipationless limit $\sigma_{xy} \gg \sigma_{xx}$, the Seebeck coefficient is given directly by Eq. (2), such that for a given charge density one need only calculate the thermodynamic entropy. The entropy per unit volume is generically given by [14,27,37]

$$n_s = -k_B \sum_n \int d\epsilon_n \nu(\epsilon_n) [f(\epsilon_n) \ln f(\epsilon_n) + (1 - f(\epsilon_n)) \ln(1 - f(\epsilon_n))], \quad (16)$$

where the sum is taken over the Landau-level index n [14,26,38]. One can view Eq. (16) as the Shannon entropy $-k_B [f \ln f + (1 - f) \ln(1 - f)]$ for a quantum state that is occupied with probability f , integrated over all quantum states. Thus, calculating the Seebeck coefficient in this high- B limit requires only knowledge of the density of states $\nu(\epsilon)$ and the Landau-level spectrum ϵ_n . In this paper, we take $\nu(\epsilon)$ to be that of the noninteracting band structure, essentially ignoring electron-electron interactions in our calculation of the entropy. This assumption fails at sufficiently low temperatures, as we discuss in Sec. V.

For the straight nodal line with magnetic field B applied along the axis of the nodal line, which is our primary consideration in this paper, the expressions for ν and ϵ_n are [14,39]

$$\epsilon_n(B) = \text{sign}(n) v_F \sqrt{2e\hbar B |n|}, \quad (17)$$

$$\nu(\epsilon) = \frac{eB}{\hbar} k_0 g \sum_n \delta(\epsilon - \epsilon_n), \quad (18)$$

where $2\pi k_0$ is the k -space length of the nodal line. (We denote the length of the nodal line as $2\pi k_0$ for reasons of notational consistency with the case of a circular nodal line considered in Sec. IV.)

III. STRAIGHT NODAL LINE

In this section, we focus on the case of an NLS with a straight nodal line. That is, we consider an electronic system with the Hamiltonian

$$H = v_F (\sigma_x p_x + \sigma_y p_y + \sigma_z F(p_z)), \quad (19)$$

where v_F is the Fermi velocity (Dirac velocity), which we take to be a constant, σ_i are the Pauli matrices, and p_i is the momentum in direction i . The nodal line resides along the p_z direction and the function $F(p_z)$ produces a variation in energy (“corrugation”) of the nodal line. For the remainder of this paper, we take $F(p_z) \equiv 0$, so that the nodal line resides at a single energy. We discuss the effects of corrugation of the nodal line in Sec. V. A schematic Fermi surface and dispersion relation are plotted in Fig. 1. The Hamiltonian (19) with $F(p_z) \equiv 0$ is equivalent to that of graphene and therefore one can think of an NLS with a straight and flat nodal line as equivalent to a stack of non-interacting 2D graphene layers. In this case, as mentioned above, only the magnetic field component in the stacking direction (z direction) has any influence on the electronic system (neglecting Zeeman coupling to the electron spin) and therefore we assume, without loss of generality, that the magnetic field $\mathbf{B} = B\hat{z}$ is aligned along the nodal line.

Before presenting results for the thermopower, we pause to discuss the physical scales associated with the problem; these are demarcated by the various regions in Fig. 2. At finite electron concentration n_e , an NLS at zero temperature has a Fermi energy $E_F = \hbar v_F k_F$, where $k_F = \sqrt{4\pi n_e / (gk_0)}$ is the Fermi wave vector. The Fermi energy sets the characteristic temperature $T_F = E_F / k_B$ of the electronic system. Thus we can first partition our parameter space by comparing T against T_F .

At low temperature $T \ll T_F$, there are two characteristic magnetic field scales: a scale B_1 at which $\omega_c(\epsilon = E_F) \tau = 1$ and a scale B_{EQL} above which only the lowest Landau level is occupied. The expression in Eq. (14) for

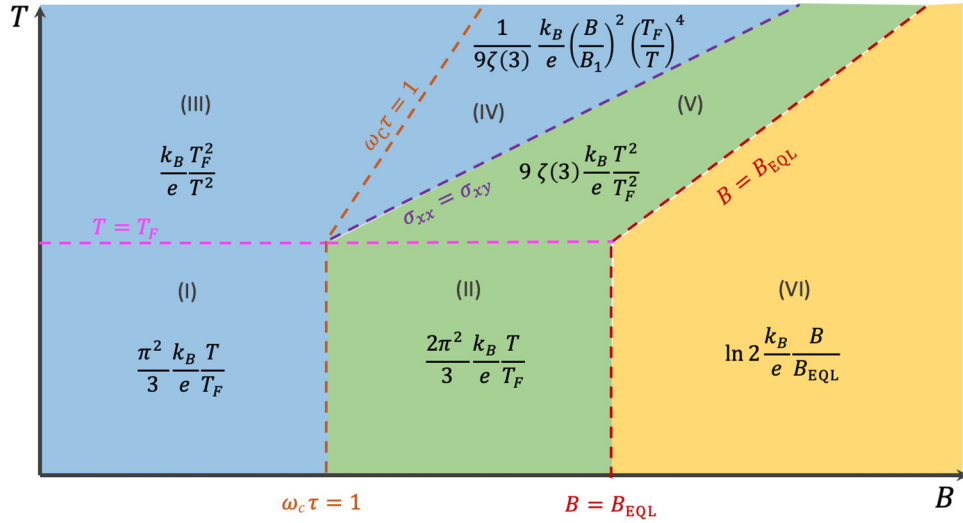


FIG. 2. A summary of the behavior of the Seebeck coefficient S_{xx} versus B and T for an NLS with a straight nodal line in various asymptotic regimes. The two axes are depicted on a logarithmic scale. The blue-shaded regions correspond to regimes in which S_{xx} is calculated using a semiclassical approach, the yellow regions correspond to regimes for which S_{xx} is calculated using the dissipationless-limit approach, and the green regions correspond to regimes in which both approaches are valid and give the same result. The various dashed lines denote the relevant temperature and magnetic field scales that define the different regimes. B_1 and B_{EQL} are defined in Eqs. (20) and (21).

the cyclotron frequency gives

$$B_1 = \frac{E_F}{ev_F^2 \tau}. \quad (20)$$

At fields $B \gg B_1$, one can think that the conductivity tensor is strongly modified from its $B = 0$ value and $\sigma_{xy} \gg \sigma_{xx}$. Calculationally, in the limit $B \gg B_1$ we can simplify the denominator of Eqs. (12) and (13) when performing asymptotic estimates of S_{ij} . The larger field scale

$$B_{\text{EQL}} = \frac{2\pi \hbar n_e}{egk_0} = \frac{E_F^2}{2e\hbar v_F^2} = B_1 \frac{E_F \tau}{\hbar} \quad (21)$$

can be identified by the condition that the degeneracy of the lowest Landau level exceeds the electron concentration. The two field scales are well separated, $B_{\text{EQL}} \gg B_1$, so long as the scattering rate $1/\tau \ll E_F/\hbar$, which is a generic requirement for having a conductor with well-defined quasiparticles. Thus at $T \ll T_F$, there are three regimes of magnetic field: a low-field regime $B \ll B_1$, an intermediate-field regime $B_1 \ll B \ll B_{\text{EQL}}$, and a high-field regime $B \gg B_{\text{EQL}}$.

At high temperatures $T \gg T_F$, both field scales B_1 and B_{EQL} are modified due to the energy dependence of ω_c and the proliferation of thermally excited holes in the valence band. Notably, the large concentration of holes implies that the Hall conductivity σ_{xy} is significantly reduced for a given field strength relative to its $T = 0$ value, since the contribution of holes to σ_{xy} has the opposite sign as the electron contribution. Thus, at $T \gg T_F$, the field

scale B_1 splits into two different values: a smaller value associated with $\omega_c(\epsilon = k_B T)\tau = 1$, since the quasiparticles have characteristic energy $\epsilon \sim k_B T$, and a larger value associated with $\sigma_{xx} = \sigma_{xy}$ [where σ_{xx} and σ_{xy} refer to the thermally averaged values of the conductivity, given by Eq. (8), and not to the values at a specific fixed energy, given by Eqs. (12) and (13)]. The smaller value associated with $\omega_c(\epsilon = k_B T)\tau = 1$ is given by $B \sim (T/T_F)B_1$, while the larger value associated with $\sigma_{xx} = \sigma_{xy}$ is given by $B \sim (T/T_F)^3 B_1$. The onset of the EQL is also delayed to $B \sim (T/T_F)^2 B_{\text{EQL}}$ at such high temperatures, since it corresponds to the condition where the Landau-level spacing is larger than $k_B T_F$ rather than E_F . Thus at $T \gg T_F$, there are four distinct regimes of magnetic field.

The different regimes of field and temperature are summarized in Fig. 2, along with the corresponding asymptotic relation for the Seebeck coefficient S_{xx} . In the remainder of this section, we summarize the behavior in each of these regimes.

A. Seebeck coefficient

We now compute the Seebeck coefficient S_{xx} across the various regimes outlined above (see Fig. 2). In the limit of low temperature $T \ll T_F$ and outside the EQL ($B \ll B_{\text{EQL}}$), which corresponds to regions (I) and (II) in Fig. 2, one can calculate the Seebeck coefficient using the usual Mott formula [Eq. (10)]. These calculations give

$$S_{xx}^{\text{I}} \simeq \frac{\pi^2 k_B T}{3 e T_F} \quad (22)$$

for the regime of $\omega_c(\epsilon = E_F)\tau \ll 1$ (small Hall angle) and

$$S_{xx}^{\text{II}} \simeq \frac{2\pi^2}{3} \frac{k_B}{e} \frac{T}{T_F} \quad (23)$$

for the regime of $\omega_c(\epsilon = E_F)\tau \gg 1$ (large Hall angle). The exact numerical prefactors in these expressions are dependent on our assumption of an energy-independent scattering time τ ; introducing a power-law dependence $\tau(\epsilon)$ would lead to different numerical prefactors to Eqs. (22) and (23) [36]. But the proportionality of the Seebeck coefficient to T/T_F is universal. One can think that this dependence arises because the electronic entropy is vanishingly small at low temperature: at low temperature, only a small fraction of electrons, proportional to T/T_F , contribute significantly to the entropy, so that the ratio of entropy to charge is also proportional to T/T_F .

At high temperatures $T \gg T_F$, there are many thermally excited electron-hole pairs, so that the total carrier density $n_e + n_h \sim k_0(k_B T)^2/(\hbar v_F)$ greatly exceeds its value at low temperature. In this way, the longitudinal conductivity σ_{xx} is greatly enhanced by temperature. The longitudinal Peltier conductivity α_{xx} , on the other hand, is greatly reduced by increased temperature. In the absence of a magnetic field, electrons and holes move in opposite directions under the presence of an electric field and consequently they carry heat in opposite directions, so that their contributions to α_{xx} cancel. Evaluating Eqs. (6) and (9) in the limit of high temperature and low magnetic field (region III in Fig. 2), one arrives at

$$S_{xx}^{\text{III}} \simeq \frac{k_B}{e} \frac{T_F^2}{T^2}. \quad (24)$$

Comparing Eqs. (22) and (24), one can see that at low magnetic field the Seebeck coefficient first increases and then decreases with temperature, achieving a maximum of order k_B/e at a temperature $T \sim T_F$. This behavior is shown in Fig. 3(a), which gives a full calculation of $S_{xx}(T)$ at low B .

As one turns on B at high temperatures $T \gg T_F$ (see Fig. 4), the electrical conductivity tensor is modified due to the Lorentz force and at sufficiently large B that $\omega_c(\epsilon = k_B T)\tau \gg 1$ it becomes strongly modified. Within this large-field limit, the distinct regimes IV and V in Fig. 2 are demarcated by whether σ_{xx} remains much larger than σ_{xy} . In regime IV, we find that

$$S_{xx}^{\text{IV}} \simeq \frac{1}{9\zeta(3)} \frac{k_B}{e} \left(\frac{B}{B_1}\right)^2 \left(\frac{T_F}{T}\right)^4, \quad (25)$$

where $\zeta(x)$ is the Riemann zeta function. Equation (25) implies a strong B^2 enhancement of the thermopower by the magnetic field. Conceptually, this strong enhancement arises because electron- and hole-type carriers are able to

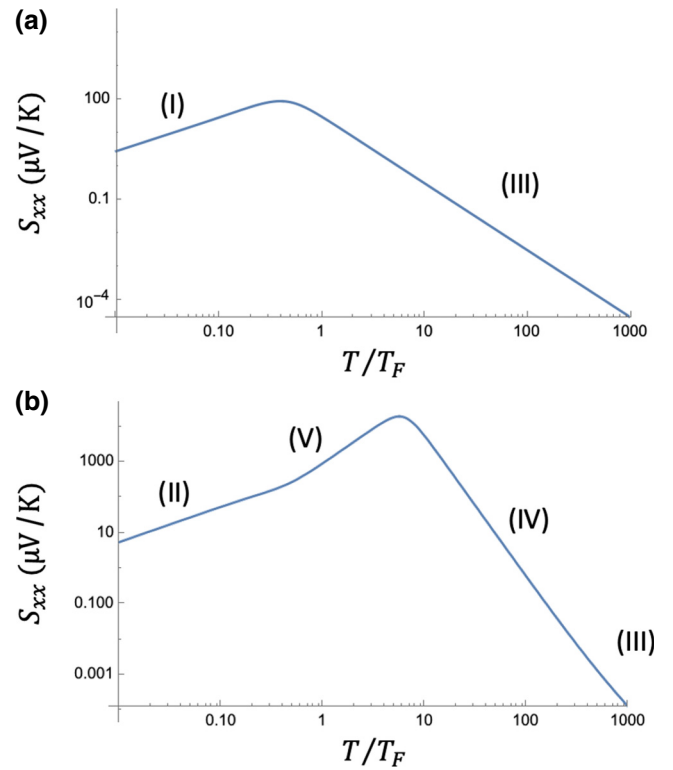


FIG. 3. (a) Variation of the Seebeck coefficient with temperature at a weak magnetic field $B = 0.1B_1$ (i.e., $\omega_c\tau \ll 1$). (b) Variation of the Seebeck coefficient with temperature at a strong magnetic field $B = 27B_1$ (i.e., $\omega_c\tau \gg 1$ at $T \ll T_F$). The results are calculated using Eqs. (6), (8), and (9).

carry heat in parallel via a longitudinal component of the $\mathbf{E} \times \mathbf{B}$ drift [35].

In regime V, where $\sigma_{xy} \gg \sigma_{xx}$ (the “dissipationless limit”), we find that

$$S_{xx}^{\text{V}} \simeq 9\zeta(3) \frac{k_B}{e} \frac{T^2}{T_F^2}. \quad (26)$$

Note that at such large fields, the Seebeck coefficient reaches a plateau value that is enormously enhanced relative to the $B = 0$ value by a factor $(T/T_F)^4$. Such a large enhancement arises due to the large Hall effect, which allows electron and hole carriers to contribute additively to the thermopower, since their motion is governed by the $\mathbf{E} \times \mathbf{B}$ drift, rather than canceling as they do at small field [13,35]. Within regime V, the thermopower increases quadratically with the temperature, arising from the strongly increasing electronic entropy. Indeed, at such large temperatures, the electron system resembles a two-component plasma with nearly equal concentrations of electrons and holes. Since the thermally populated density of carriers $n_e + n_h$ increases as T^2 , the Seebeck coefficient does as well. The strong enhancement of S_{xx} by the magnetic field is shown in Figs. 3(b) and 4(b).

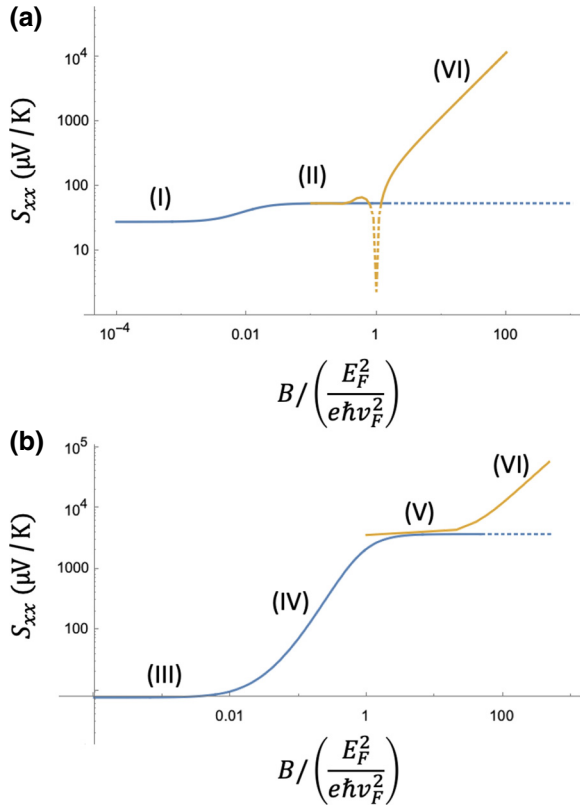


FIG. 4. (a) Variation of the Seebeck coefficient with the magnetic field at a low temperature $T = 0.1T_F$. The unit of the magnetic field on the x axis is equal to $2B_{\text{EQL}}$. (b) Variation of the Seebeck coefficient with the magnetic field at a high temperature $T = 2T_F$. The blue lines in this plot (regimes I, II, III, IV, and V) are calculated using the semiclassical approach of Eqs. (6), (8), and (9), while the yellow lines (regimes II, V and VI) correspond to the dissipationless-limit calculation [Eqs. (2) and (16)]. In both plots, the value of the momentum relaxation time is taken to be $\tau = 100\hbar/E_F$.

For sufficiently large $B \gg B_{\text{EQL}}$, only one (dispersionless) Landau level is occupied. At $B \gg B_{\text{EQL}}$, this lowest Landau level approaches half-filling, since it is electron-hole degenerate and the hole states are filled. Thus, S_{xx} is completely determined by the configurational entropy associated with half-filling a highly degenerate Landau level [e.g., Eq. (2)]. Using the Landau-level degeneracy $N_{\text{flat}} = gk_0/l_B^2$ per volume, we can write the entropy density:

$$n_s = k_B \ln \left(\frac{N_{\text{flat}}}{2} \right) \simeq k_B N_{\text{flat}} \ln 2 = k_B \frac{gk_0}{l_B^2} \ln 2. \quad (27)$$

Here, $l_B = \sqrt{\hbar/(eB)}$ is the magnetic length. Since the entropy scales linearly with B , it is clear that the Seebeck coefficient scales as $S_{xx} \propto B$, with no T dependence. More

explicitly, we have

$$S_{xx}^{\text{VI}} \simeq 2 \ln 2 \frac{k_B}{e} \frac{ev_F^2 \hbar}{E_F^2} B = \ln 2 \frac{k_B}{e} \frac{B}{B_{\text{EQL}}}. \quad (28)$$

The strong enhancement of S_{xx} upon entering the EQL is shown in Fig. 4. The brief sharp dip in $S_{xx}(B)$ that can be seen in Fig. 4(a) at $B \sim B_{\text{EQL}}$ arises because of a suppression of the electronic entropy when the chemical potential lies in the gap between the lowest and second-lowest Landau levels. We note that in deriving Eq. (28), we have implicitly assumed that the density of states is well described by a noninteracting electron picture (as mentioned in Sec. II C). At sufficiently low temperatures, this assumption becomes invalidated due to exchange splitting of the lowest Landau level. We discuss this issue in Sec. V.

B. Nernst coefficient

Let us now summarize the behavior of the Nernst coefficient S_{xy} as a function of T and B . We limit our discussion here to the semiclassical regime, in which S_{xy} can be computed using Eqs. (7)–(9). Unlike the Seebeck coefficient, the Nernst coefficient is not well defined in the dissipationless limit $\tau \rightarrow \infty$, since the value of S_{xy} always depends on a longitudinal electrical or thermoelectric conductivity [σ_{xx} or α_{xx} ; see Eq. (7)]. Such longitudinal conductivities cannot be defined without reference to a momentum relaxation mechanism (unlike Hall conductivities, which remain finite even when there is no scattering due to the $\mathbf{E} \times \mathbf{B}$ drift of carriers). However, we show here that the peak value of the Nernst coefficient arises at fields corresponding to $\sigma_{xy} \sim \sigma_{xx}$, which are well below B_{EQL} . Thus, increasing B into the EQL does not provide additional benefit for the Nernst effect.

At low temperature $T \ll T_F$ and within the semiclassical regime, $B \ll B_{\text{EQL}}$, we can again apply the Mott formula [Eq. (10)]. This calculation gives

$$S_{xy}^{\text{I}} \simeq \frac{\pi^2}{3} \frac{k_B}{e} \frac{B}{B_1} \frac{T}{T_F} \quad (29)$$

for the regime of $\omega_c(\epsilon = E_F)\tau \ll 1$ (small Hall angle) and

$$S_{xy}^{\text{II}} \simeq \frac{\pi^2}{3} \frac{k_B}{e} \frac{B_1}{B} \frac{T}{T_F} \quad (30)$$

for the regime of $\omega_c(\epsilon = E_F)\tau \gg 1$ (large Hall angle). Thus, the Nernst coefficient achieves a peak value $S_{xy} \sim (k_B/e)(T/T_F)$ at a field $B \sim B_1$.

At high temperatures $T \gg T_F$, we must again consider the coexistence of thermally excited electrons and holes. For small enough fields that $\omega_c(\epsilon = k_B T)\tau \ll 1$, we find

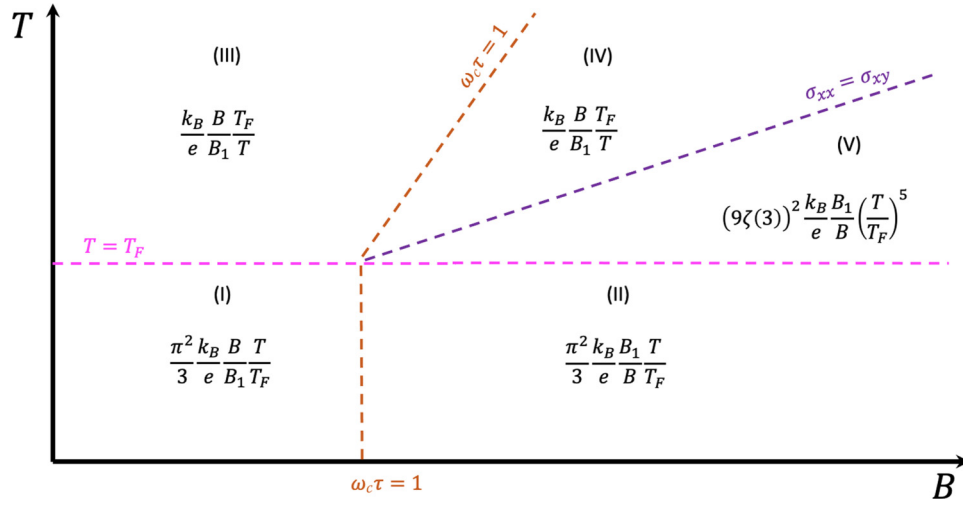


FIG. 5. A schematic diagram showing asymptotic expressions for the Nernst coefficient S_{xy} within different regimes of temperature and magnetic field. The labels for each regime are the same as in Fig. 2. The magnetic field scale B_1 is defined by Eq. (20).

that

$$S_{xy}^{\text{III}} \simeq \frac{k_B B T_F}{e B_1 T}. \quad (31)$$

As the magnetic field is increased, this linear increase of S_{xy} with B continues uninterrupted until sufficiently large fields that $\sigma_{xy} \sim \sigma_{xx}$. In other words,

$$S_{xy}^{\text{IV}} = S_{xy}^{\text{III}} \simeq \frac{k_B B T_F}{e B_1 T}. \quad (32)$$

At large enough fields that $\sigma_{xy} \gg \sigma_{xx}$, the value of S_{xy} declines again with B according to

$$S_{xy}^{\text{V}} \simeq (9\zeta(3))^2 \frac{k_B B_1}{e B} \left(\frac{T}{T_F}\right)^5. \quad (33)$$

These results imply that at $T \gg T_F$, the maximum in S_{xy} is not achieved at $B \sim B_1$; instead, the linear-in- B growth of the Nernst coefficient is continued to a much larger field, $B \sim (T/T_F)^3 B_1$. Correspondingly, the maximum value of the Nernst coefficient is not of order k_B/e but is much larger: $S_{xy}^{\text{(max)}} \sim (k_B/e)(T/T_F)^2$. This large enhancement of the peak Nernst coefficient by the magnetic field is reminiscent of a similar effect in conventional semimetals [35].

The different regimes of behavior for the Nernst coefficient are summarized in Fig. 5.

IV. CIRCULAR NODAL LINE

In this section, we consider the applicability of our results to the case in which the conduction and valence bands meet at a circle in momentum space rather than a straight line. Such (approximately) circular nodal lines

appear in materials such as ZrSiS [40], HfSiS [41], and Ca_3P_2 [42]. One model Hamiltonian for describing a circular nodal line in the k_x - k_z plane is [43,44]

$$H = \frac{\hbar^2}{2m}(k_x^2 + k_z^2 - k_0^2)\sigma_x + \hbar v_F k_y \sigma_y, \quad (34)$$

where k_0 is the radius of the nodal line in reciprocal space. The corresponding conduction and valence bands have a linear dispersion for momenta close to the nodal line, with a Fermi velocity v_F in the y direction (perpendicular to the nodal line) and a velocity $v_{\parallel} = \hbar k_0/m$ in the x and z directions (within the plane of the nodal line). The corresponding Fermi surface at finite E_F is depicted in Fig. 6. Throughout this section, we assume that $E_F, k_B T \ll \hbar^2 k_0^2/m$, so that the Fermi surface takes the shape of a thin torus.

We note that, in general, the nodal line in real materials is not constrained to reside at a single energy. The ‘‘corrugation’’ of the nodal line provides an additional energy

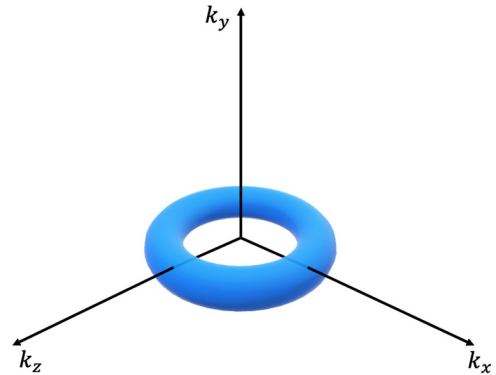


FIG. 6. A schematic of the Fermi surface of an NLS with a circular nodal line in the k_x - k_z plane.

scale that is not within our description. Thus the results that we derive here are applicable when either E_F or $k_B T$ is much larger than the corrugation of the nodal line in energy. We discuss this assumption further in Sec. V.

Let us now consider the behavior of the Seebeck coefficient as a function of the magnetic field. We first consider the case in which \mathbf{B} is in the x - z nodal-line plane; without loss of generality, we take $\mathbf{B} = B\hat{z}$. Since the Lorentz force does not act on currents in the \hat{z} direction, we do not expect S_{zz} to be modified from its zero-field value and thus the Seebeck coefficient follows either Eqs. (22) or (24), depending on whether T is large or small compared to T_F . The thermopowers S_{xx} and S_{yy} along the directions orthogonal to \mathbf{B} , on the other hand, do exhibit a magnetic field enhancement. For S_{xx} , the dominant contribution to thermoelectric transport arises from regions of the Fermi surface that have a high velocity along the x direction. These are the regions in which the nodal ring is nearly parallel to \mathbf{B} . Since the Fermi surface is locally cylindrical, the behavior of the thermopower reduces to an analogue of the straight-nodal-line case considered in Sec. III, with some ‘‘effective length’’ of the nodal line that is of order k_0 [45]. Correspondingly, we expect $S_{xx}(B)$ to match the behavior outlined in Fig. 2 up to order-1 numerical prefactors. For the thermopower S_{yy} along the y direction, the entirety of the nodal line is strongly dispersive along the y direction but only those parts of the Fermi surface that are nearly parallel to \mathbf{B} experience a significant Lorentz force. For such regions, the thermopower is again similar to what is shown in Fig. 2. So we arrive at the conclusion that both $S_{xx}(B)$ and $S_{yy}(B)$ are equivalent to the case of the straight nodal line up to numerical prefactors. (We are neglecting in our discussion the effects of weak localization, which can provide a correction to the conductivity tensor at low magnetic field that is strongly dependent on the field direction [45].)

Let us consider in detail the behavior of the Seebeck coefficient in the EQL (regime VI). For the case of a straight nodal line, the large linear-in- B and temperature-independent value of S_{xx} [Eq. (28)] arises from the existence of a zero-energy Landau level that is shared by conduction- and valence-band states and that does not disperse along the field direction. In fact, the circular nodal line also exhibits a zero-energy Landau level that is dispersionless for k_z in the range $-k_0 < k_z < k_0$ (see Fig. 7); this result has been derived in Refs. [31,46,47]. We also provide a detailed derivation of the Landau-level spectrum in Appendix B. The dispersionless portion of the zero-energy Landau level enables a Seebeck coefficient enhancement that is very similar to that of Eq. (28).

Quantitatively, we can estimate the value of $S_{xx}(B)$ at $B \gg B_{\text{EQL}}$ by assuming that carriers half-populate the flat portion of the $n = 0$ Landau level. At temperatures that are low compared to $\sqrt{\hbar^2 v_F k_0 e B / m}$ (the spacing between the zeroth and first Landau levels at small k_z),

the configurational entropy of carriers within this flat portion of the zeroth Landau level provides the primary contribution to the entropy. The degeneracy of the flat band is $N_{\text{flat}} = g k_0 / (\pi l_B^2)$ per volume, where $l_B = \sqrt{\hbar / e B}$ is the magnetic length. The flat band is half-filled and therefore the entropy density is

$$n_s = k_B \ln \left(\frac{N_{\text{flat}}}{2} \right) \simeq k_B N_{\text{flat}} \ln 2 = k_B \frac{g k_0}{\pi l_B^2} \ln 2. \quad (35)$$

The charge density is given by

$$\rho_e = e g \frac{\pi k_{F\perp} k_{F\parallel} \cdot (2\pi k_0)}{(2\pi)^3} = \frac{g m E_F^2 e}{4\pi \hbar^3 v_F}. \quad (36)$$

Here, the numerator in the first equality of Eq. (36) represents the volume of the toroidal Fermi surface, with $k_{F\perp}$ and $k_{F\parallel}$ being the Fermi momentum in the directions perpendicular (y direction) and parallel (x - z plane) to the circular nodal line, respectively. Note that the toroidal Fermi surface need not have circular cross section. In the second equality, we use the relations $E_F = \hbar v_F k_{F\perp} = \hbar v_{\parallel} k_{F\parallel}$, where E_F is the energy measured relative to the nodal line. Thus, we find that

$$S_{xx}^{\text{VI}} \simeq 4 \ln 2 \frac{k_B e \hbar^2 v_F k_0}{e m E_F^2} B. \quad (37)$$

As argued above, we recover the large linear-in- B and temperature-independent behavior of the Seebeck coefficient obtained for the case of a straight nodal line. In fact, one can obtain this result directly from Eq. (28) by making the simple replacement $v_F^2 \rightarrow v_{\parallel} v_F$ and inserting an additional factor of 2 associated with the fact that occupied states range from $-k_0$ to k_0 .

Finally, let us consider the case in which $\mathbf{B} = B\hat{y}$ is applied out of the nodal-line plane. At zero magnetic field,

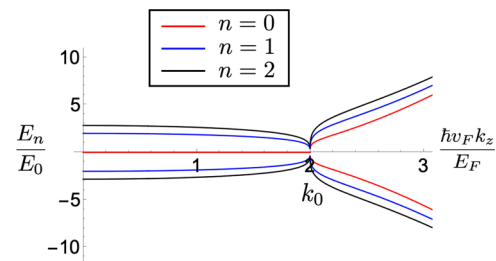


FIG. 7. The dispersion relation for the lowest three Landau levels of an NLS with a circular nodal line in the k_x - k_z plane, plotted as a function of the momentum k_z along the field direction [using Eqs. (B33) and (B36)]. This example uses $k_0 = 2E_F / (\hbar v_F)$. The unit of energy on the y axis, $E_0 = \sqrt{\hbar^2 e B v_F k_0 / m} = \hbar (v_F v_{\parallel})^{1/2} / l_B$. Note that the zeroth Landau level (red curve) is dispersionless and electron-hole degenerate for $|k_z| < k_0$.

the thermopower is identical to the case of the straight nodal line, since the Fermi surface is everywhere locally cylindrical. Significant magnetic field effects appear only when $\omega_c \tau$ becomes order-1 or larger, where in this case the value of ω_c depends on the mass associated with cyclotron motion in the x - z plane. For such motion, the effective mass is of order m [where the parameter m is defined by the Hamiltonian given in Eq. (34)], rather than the much smaller effective mass associated with “out-of-plane” cyclotron motion: $m_{\perp} \equiv \hbar k_F / v_F$. When $m_{\perp} / m \sim \hbar \sqrt{n_e} / (v_F m \sqrt{k_0}) \ll 1$, i.e., for sufficiently large k_0 or low electron concentration, the strength of an out-of-plane B field necessary to produce significant magnetic field effects is much larger than for the in-plane case. For example, an NLS with charge density $n = 10^{18} \text{ cm}^{-3}$, Fermi velocity $v_F \sim 10^5 \text{ m/s}$, and nodal-line radius $k_0 \sim 0.1 \text{ \AA}^{-1}$ would have $m_{\perp} / m \sim 0.03$, so that producing strong magnetic effects by an out-of-plane magnetic field would require a 30-times-larger field than for the case of an in-plane magnetic field. We therefore leave the case of out-of-plane field to be explored by future work.

V. SUMMARY AND OUTLOOK

We have studied the behavior of the thermoelectric coefficients of nodal-line semimetals across all regimes of temperature and magnetic field. Our results broadly apply regardless of the shape of the nodal line, as discussed in Sec. IV. We find that a magnetic field produces a large enhancement of both the Seebeck and Nernst coefficients, as depicted in Figs. 2–5, so that both can be driven well above k_B/e .

It should be emphasized that it is usually difficult in conducting materials to achieve a thermopower that is parametrically enhanced above the natural unit $k_B/e \approx 86 \mu\text{V/K}$ within the metallic state, due to the fundamental trade-off between having low electronic entropy at low temperature and having cancellation between electron and hole contributions to thermal transport at high temperature. But a strong magnetic field is able to circumvent this limitation by enabling a transverse mechanism of thermoelectric transport in which electrons and holes carry heat in parallel via the $\mathbf{E} \times \mathbf{B}$ drift [13]. Some preliminary evidence for this strong magnetic field enhancement has been seen in the NLS Mg_3Bi_2 [48].

Our most dramatic finding is that at a sufficiently large magnetic field that only the lowest Landau level is occupied, i.e., in the extreme quantum limit, an NLS exhibits a large linear-in- B and temperature-independent Seebeck coefficient, as given by Eq. (28). This large thermopower arises fundamentally from the huge entropy associated with a half-filled and electron-hole degenerate lowest Landau level, which is a hallmark of topological semimetals. As we discussed in Sec. IV, this feature exists for both straight and circular nodal lines. Given the simplicity of

this result, it is worth writing Eq. (28) in experimental units:

$$S_{xx}^{\text{VI}} \simeq 289 \mu\text{V/K} \times \frac{(k_0 [\text{in } \text{\AA}^{-1}])(B [\text{in T}])}{n_e [\text{in } 10^{18} \text{ cm}^{-3}]}. \quad (38)$$

In this expression, $2\pi k_0$ corresponds to the length of the nodal line. Note that even under very realistic experimental conditions, such as $k_0 \sim 0.1 \text{ \AA}^{-1}$, $B = 10 \text{ T}$, and $n_e = 10^{18} \text{ cm}^{-3}$, it becomes possible to attain a large thermopower $S_{xx} \approx 300 \mu\text{V/K}$ even at very low temperature. Under more optimistic conditions, where the carrier concentration is reduced significantly below 10^{18} cm^{-3} , it may be possible to realize thermopower on the order of mV/K at low temperature.

It should be noted that for most practical applications, the thermodynamic efficiency is determined not by the Seebeck coefficient alone but by the thermoelectric figure of merit $zT = S_{xx}^2 T / \rho \kappa$, which depends on the electrical resistivity ρ and the thermal conductivity κ . (In the presence of a magnetic field, both ρ and κ are tensors but this expression for the figure of merit remains accurate with the substitutions $\rho \rightarrow \rho_{xx}$ and $\kappa \rightarrow \kappa_{xx}$ so long as $\kappa_{xy} \ll \kappa_{xx}$ [13].) In materials with low Fermi energy, κ is dominated by phonons at all but extremely small temperatures, while the resistivity ρ_{xx} may be subject to strong and nontrivial magnetoresistance effects. Calculating these quantities is therefore beyond the scope of this paper. However, we note that within the EQL (regime VI) one can write the figure of merit as

$$zT \simeq 0.36 \frac{(B/B_{\text{EQL}})^2}{(\kappa_{xx}/T [\text{in } \text{Wm}^{-1}\text{K}^{-2}])(\rho_{xx} [\text{in } \mu\Omega\text{cm}])}. \quad (39)$$

The quantities in the denominator of this expression can realistically be of order unity (e.g., in ZrSiS [49,50]). Achieving large zT at low temperature therefore seems plausible if the EQL can be achieved or, in other words, if the magnetic field is strong enough and the level of unintentional doping is sufficiently low. Of course, practical applications will also require reducing the field scale B_{EQL} to the level that can be achieved by a permanent magnet (below 1–2 T), so that additional power input is not required to generate the magnetic field.

So far, we have assumed the nodal line to be flat in energy, meaning that we neglect variations in energy along the nodal line (“corrugations” of the nodal line). In general, there is no symmetry that constrains a nodal line to reside at constant energy [e.g., the function $F(p_z)$ in Eq. (19) need not be zero], and any such variation introduces an additional energy scale that competes with the magnetic field effects we are discussing. Specifically, when the Fermi energy is small compared to the corrugation energy scale, the toroidal Fermi surface depicted in Fig. 6 breaks up into contiguous electron and hole pockets. Such an effect is

apparently prominent in ZrSiS, for example [40,51], and it puts a lower limit on the achievable carrier density that is apparently of order $n_e \sim 10^{19} \text{ cm}^{-3}$ [49,52]. Practical efforts to achieve low-temperature thermoelectrics using NLSs may therefore find it fruitful to identify materials with a nearly flat nodal line.

Finally, we mention that throughout this paper, we have worked within a noninteracting band picture, ignoring the effects of electron-electron interactions. Such a picture is not generally applicable in a flat band at very low temperature, since the exchange interaction tends to split a degenerate band into spin- or orbital-polarized subbands. For example, 2D graphene has a zero-energy Landau level that is nominally fourfold degenerate, but at liquid helium temperatures and high fields this Landau level is split by the exchange interaction into spin- and valley-polarized subbands [53]. This exchange splitting limits the entropy of the electron system and bounds the measured Seebeck coefficient at just a few times k_B/e [54]. Whether such exchange splitting is relevant for 3D NLSs remains to be seen but if it is relevant, then its primary effect will be to limit the applicability of our results to temperatures above the exchange-splitting scale.

ACKNOWLEDGMENTS

We thank Mingda Li for helpful discussions. This work was primarily supported by the Center for Emergent Materials, a National Science Foundation (NSF) -funded Materials Research Science and Engineering Center (MRSEC), under Grant No. DMR-2011876. G.B. is supported by the U.S. Department of Energy (DOE) Established Program to Stimulate Competitive Research (EPSCoR) via Grant No. DE-SC0024284.

APPENDIX A: COMMENTS ON THE CHEMICAL POTENTIAL

Throughout the main text, we have assumed that the charge density $n_e - n_h$ of carriers within the nodal-line bands remains constant as a function of the magnetic field and the temperature. This assumption is natural if there are no other electron bands within approximately $k_B T$ of the Fermi level. Using this assumption, we can calculate the dependence of the chemical potential on temperature using Eq. (11), which gives the result shown in Fig. 8. At low temperature, the value of μ approaches E_F , while at high temperatures $T \gg E_F$, we have $\mu \simeq E_F^2 / (4k_B T \ln 2)$.

On the other hand, if there are other bands with a high density of states intersecting the chemical potential, then these bands can have the effect of pinning the value of μ so that it does not evolve (or evolves more weakly) as a function of temperature. Such a situation apparently arises in, e.g., the Dirac semimetal ZrTe₅ [16] and in the Weyl

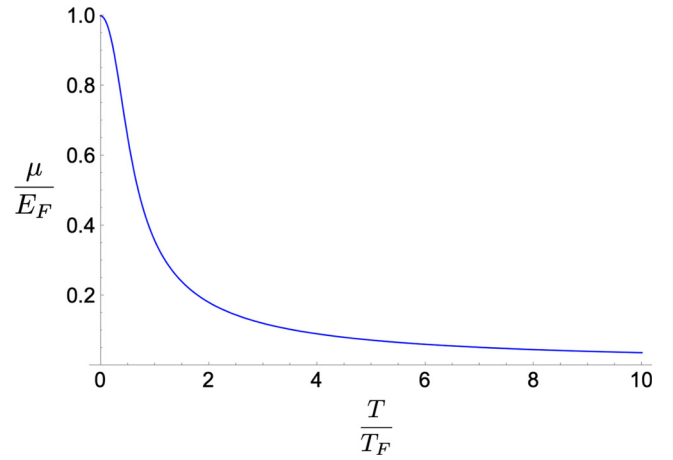


FIG. 8. The chemical potential μ as a function of temperature T for the case of fixed charge density in the nodal-line bands.

semimetal NbP [15]. Thus, it is worth briefly considering how our results are modified in the case in which μ is constant as a function of temperature.

In Figs. 9 and 10, we show the corresponding values of the Seebeck and Nernst coefficients for the case in which μ is constant as a function of temperature. In general, the expressions are unmodified at low temperatures $T \ll T_F$, since in this case the chemical potential μ approaches E_F in any situation. The value of S_{xx} is also unchanged in the EQL (regime VI, not shown in Figs. 9 and 10). At higher temperatures $T \gg T_F$, the power-law dependence on the temperature is modified due to the chemical potential not sinking down toward the nodal line at higher temperatures, although the qualitative dependence on T remains the same

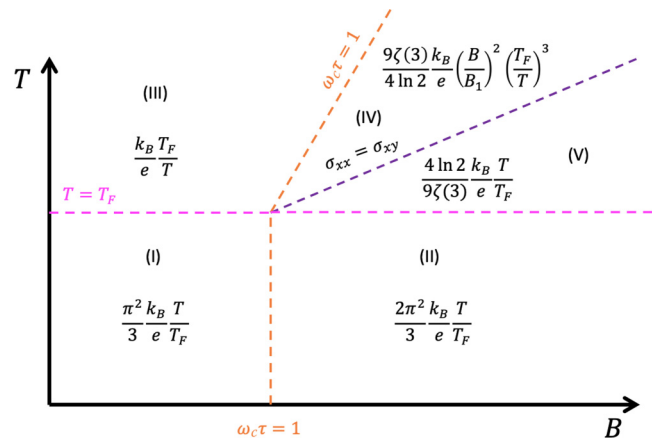


FIG. 9. A summary of the behavior of the Seebeck coefficient S_{xx} versus B and T for an NLS with a straight nodal line in various asymptotic regimes, assuming a constant chemical potential μ as a function of T . The two axes are depicted on a logarithmic scale and the various regimes of T and B are the same as in Fig. 2. B_1 is as defined in Eq. (20).

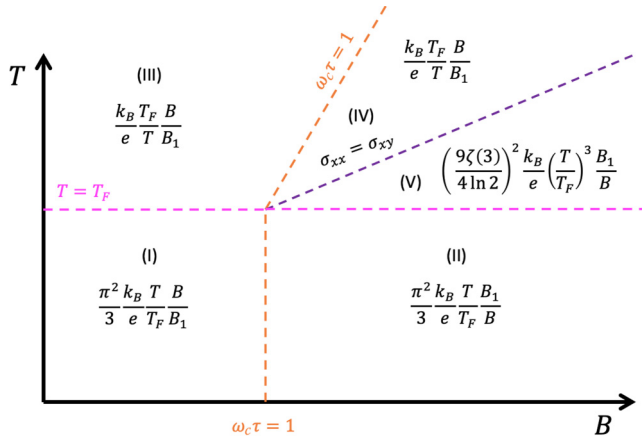


FIG. 10. A summary of the behavior of the Nernst coefficient S_{xy} versus B and T for an NLS with a straight nodal line in various asymptotic regimes, assuming a constant chemical potential μ as a function of T . The two axes are depicted on a logarithmic scale and the various regimes of T and B are the same as in Fig. 5. B_1 is as defined in Eq. (20).

in all regimes. The power-law dependence of both S_{xx} and S_{xy} to B is unchanged in all regimes.

APPENDIX B: LANDAU LEVELS OF A CIRCULAR NODAL LINE

The Hamiltonian for electron bands near a circular nodal line is given by Eq. (34). The first term describes the circular nodal line in the momentum space, with the radius k_0 . The second term describes the linear dispersion in the k_z direction. σ_x and σ_y are the Pauli matrices.

We assume the magnetic field to be oriented in the plane parallel to the plane of the nodal line and in the z direction. We can introduce this field using a Peierls substitution $p_y \rightarrow \hbar k_y - eBx$, so that the Hamiltonian can be written as

$$H = \frac{\hbar^2}{2m}(k_z^2 - k_0^2 - \partial_x^2)\sigma_x + v_F(\hbar k_y - eBx)\sigma_y. \quad (\text{B1})$$

1. Zero-energy modes

We begin by calculating the eigenstates with zero energy. By substitution, and solving the Schrodinger equation, we find that the possible solutions exist only when $p_x < p_0$. Multiplying out the matrix given in Eq. (B1) for a wave function $(\psi_1, \psi_2)^T$, we arrive at

$$\left[\frac{1}{2m}(p_z^2 - p_0^2 - \hbar^2 \partial_x^2) + iv_F(p_y - eBx) \right] \psi_1 = 0, \quad (\text{B2})$$

$$\left[\frac{1}{2m}(p_z^2 - p_0^2 - \hbar^2 \partial_x^2) - iv_F(p_y - eBx) \right] \psi_2 = 0. \quad (\text{B3})$$

To solve for ψ_2 , we rewrite the equation as

$$\hbar^2 \partial_x^2 \psi_2 = 2miv_F eB \left(x - \frac{p_y}{eB} + \frac{p_z^2 - p_0^2}{2imv_F eB} \right) \psi_2. \quad (\text{B4})$$

Using the new variable

$$x' = x - \frac{p_y}{eB} + \frac{p_z^2 - p_0^2}{2imv_F eB}, \quad (\text{B5})$$

this equation becomes

$$\hbar^2 \frac{\partial^2 \psi_2}{\partial x'^2} = 2miv_F eB x' \psi_2. \quad (\text{B6})$$

Introducing another new variable, $z = (2miv_F eB/\hbar^2)^{1/3} x'$, the equation turns into the Airy equation:

$$\frac{\partial^2 \psi_2}{\partial z^2} = z \psi_2. \quad (\text{B7})$$

The solution to this equation is the Airy function

$$\psi_2 = \text{Ai}(z). \quad (\text{B8})$$

Coming back to the original variable,

$$\psi_2 = \text{Ai} \left(\left(\frac{2imv_F eB}{\hbar^2} \right)^{1/3} \left(x - \frac{p_y}{eB} + \frac{p_z^2 - p_0^2}{2imv_F eB} \right) \right). \quad (\text{B9})$$

Using the asymptotic expression for Airy functions as the argument $z \rightarrow \infty$,

$$\text{Ai}(z) \simeq \frac{\exp \left[-\frac{2}{3} z^{3/2} \right]}{2\sqrt{\pi} z^{1/4}}, \quad (\text{B10})$$

we obtain

$$\psi_2 \simeq \frac{\exp \left[-\frac{2}{3} (2imv_F eB/\hbar^2)^{1/2} \left(x - \frac{p_y}{eB} + \frac{p_z^2 - p_0^2}{2imv_F eB} \right)^{3/2} \right]}{2\sqrt{\pi} (2imv_F eB/\hbar^2)^{1/12} \left(x - \frac{p_y}{eB} + \frac{p_z^2 - p_0^2}{2imv_F eB} \right)^{1/4}}. \quad (\text{B11})$$

In the limit $x \rightarrow \infty$, this expression decays exponentially.

Now, we shall study the behavior of the wave function when the x variable changes from ∞ to $-\infty$ and therefore when the argument z of the Airy function changes from $e^{i\pi/6}\infty$ to $e^{-5i\pi/6}\infty$ or $e^{7i\pi/6}\infty$. For $p_z > p_0$, in the complex plane y lies below zero; to obtain a continuous expression, we assume at $x \rightarrow -\infty$, $z \rightarrow e^{-5i\pi/6}\infty$, and therefore $z^{3/2} \rightarrow e^{-5i\pi/4}\infty$. For $p_z < p_0$, in the complex plane x lies below zero; to obtain a continuous expression,

we assume at $x \rightarrow -\infty$, $z \rightarrow e^{(7i\pi/6)}\infty$, and therefore $z^{3/2} \rightarrow e^{7i\pi/4}\infty$. Therefore, at $x \rightarrow -\infty$, ψ_2 only decays at $p_z < p_0$.

The calculation for ψ_1 is very similar to the calculation for ψ_2 . The equation is as follows:

$$\hbar^2 \partial_x^2 \psi_1 = -2miv_F eB \left(x - \frac{p_y}{eB} + \frac{p_z^2 - p_0^2}{-2imv_F eB} \right) \psi_1. \quad (\text{B12})$$

Similarly, we declare a new variable,

$$x' = x - \frac{p_y}{eB} + \frac{p_z^2 - p_0^2}{-2imv_F eB}, \quad (\text{B13})$$

and the equation becomes

$$\hbar^2 \frac{\partial^2 \psi_1}{\partial x'^2} = -2miv_F eB x' \psi_1. \quad (\text{B14})$$

Introducing a new variable $z = (-2miv_F eB / \hbar^2)^{1/3} x'$, the equation turns into Airy equation:

$$\frac{\partial^2 \psi_1}{\partial z^2} = z \psi_1. \quad (\text{B15})$$

The solution of this equation is

$$\psi_1 = \text{Ai}(z) \sim \frac{e^{-\frac{2}{3}z^{3/2}}}{2\sqrt{\pi}z^{1/4}}. \quad (\text{B16})$$

At the limit $x \rightarrow \infty$, $z^{3/2} \sim e^{-i\pi/4}$, this expression decays exponentially. At the limit $x \rightarrow -\infty$, $z^{3/2} \sim e^{-7i\pi/4}\infty$ for $p_z < p_0$ and $z^{3/2} \sim e^{5i\pi/4}\infty$ at $p_z > p_0$. So we conclude that zero modes exist only at $p_z < p_0$.

2. Solutions with nonzero energies

a. Preliminary steps

In order to calculate the non-zero-energy eigenstates, we first write the wave function in terms of its Fourier transform:

$$\psi_{1(2)}(p_z, p_y, x) = \int \frac{dp_x}{2\pi\hbar} e^{ip_x x / \hbar} \psi_{1(2)}(p_x, p_y, p_z). \quad (\text{B17})$$

The \hat{x} operator transforms as $\hat{x} \rightarrow i\hbar(\partial/\partial p_x)$. The Hamiltonian in momentum representation can be written as

$$H = \frac{1}{2m} (p_x^2 + p_z^2 - p_0^2) \sigma_x + v_F \left(p_y - ieB\hbar \frac{\partial}{\partial p_x} \right) \sigma_y. \quad (\text{B18})$$

We introduce a change of variables,

$$\psi_{1(2)}(p) = e^{-ip_x p_y / eB\hbar} \phi_{1(2)}, \quad (\text{B19})$$

so that the eigenvalue problem $H\psi = E\psi$ looks like

$$\frac{E}{v_F eB} \begin{pmatrix} \phi_1 \\ \phi_2 \end{pmatrix} = \begin{pmatrix} 0 & A^\dagger \\ A & 0 \end{pmatrix} \begin{pmatrix} \phi_1 \\ \phi_2 \end{pmatrix}. \quad (\text{B20})$$

Here, A and A^\dagger are defined as

$$A = \hbar \frac{\partial}{\partial p_x} + \frac{p_x^2 + p_z^2 - p_0^2}{2mv_F eB}, \quad (\text{B21})$$

$$A^\dagger = -\hbar \frac{\partial}{\partial p_x} + \frac{p_x^2 + p_z^2 - p_0^2}{2mv_F eB}. \quad (\text{B22})$$

The corresponding eigenvalues and eigenfunctions can be solved using the following equations:

$$\left(\frac{E}{v_F eB} \right)^2 \phi_1 = A^\dagger A \phi_1, \quad (\text{B23})$$

$$\left(\frac{E}{v_F eB} \right)^2 \phi_2 = A A^\dagger \phi_2. \quad (\text{B24})$$

The explicit forms of the operators on the right-hand side are

$$A^\dagger A = -\hbar^2 \frac{\partial^2}{\partial p_x^2} + \frac{(p_x^2 + p_z^2 - p_0^2)^2}{(2mv_F eB)^2} - \frac{\hbar p_x}{mv_F eB}, \quad (\text{B25})$$

$$A A^\dagger = -\hbar^2 \frac{\partial^2}{\partial p_x^2} + \frac{(p_x^2 + p_z^2 - p_0^2)^2}{(2mv_F eB)^2} + \frac{\hbar p_x}{mv_F eB}. \quad (\text{B26})$$

In the remainder of this subsection, we derive solutions to these eigenvalue equations for the separate cases in which the momentum $|p_z| < p_0$ and $|p_z| > p_0$.

b. $|p_z| < p_0$

We now evaluate the energy levels for the case in which $|p_z| < p_0$. The Schrodinger equation in this case is given by

$$\left(\frac{E}{v_F eB} \right)^2 \phi_2 = \left[-\hbar^2 \frac{\partial^2}{\partial p_x^2} + V(p_x) \right] \phi_2, \quad (\text{B27})$$

where

$$V(p_x) = \frac{(p_x^2 + p_z^2 - p_0^2)^2}{(2mv_F eB)^2} + \frac{\hbar p_x}{mv_F eB} \quad (\text{B28})$$

plays the role of a ‘‘potential’’ in momentum space. The potential $V(p_x)$ has the form of a ‘‘Mexican-hat’’ potential, with two degenerate minima as a function of p_x , located at

$$p_x = \pm \sqrt{p_0^2 - p_z^2} - \frac{\hbar mv_F eB}{2(p_0^2 - p_z^2)}. \quad (\text{B29})$$

Expanding the potential around these minima and using the limit $4m\hbar v_F eB \ll (p_z^2 - p_0^2)^{3/2}$, the potential can be

written as

$$V(p_x) \approx \pm \frac{\sqrt{p_0^2 - p_z^2}}{\hbar^2 m v_F e B} + \frac{p_0^2 - p_z^2}{(\hbar m v_F e B)^2} (\delta p_x)^2, \quad (\text{B30})$$

where δp_x is given by

$$\delta p_x = p_x - \left[\pm \sqrt{p_0^2 - p_z^2} - \frac{\hbar m v_F e B}{2(p_0^2 - p_z^2)} \right]. \quad (\text{B31})$$

We justify our assumption of small δp_x below.

Equation (B30) implies that the Schrodinger equation becomes that of a 1D harmonic oscillator, which gives us the following energy eigenvalues:

$$E = \pm (p_0^2 - p_z^2)^{1/4} \sqrt{\frac{2\hbar v_F e B (n+1)}{m}}, \quad (\text{B32})$$

for the minima denoted by “+” and

$$E = \pm (p_0^2 - p_z^2)^{1/4} \sqrt{\frac{2\hbar v_F e B n}{m}} \quad (\text{B33})$$

for the minima denoted by “-”. In both cases, the integer $n = 0, 1, 2, \dots$. This latter equation implies the existence of a zero-energy Landau level at $p_z < p_0$.

c. $|p_z| > p_0$

We now calculate the energy values for the case $|p_z| > p_0$. If we assume again that δp_z is small enough that $4m\hbar v_F e B \ll (p_z^2 - p_0^2)^{3/2}$, then we arrive at a parabolic potential $V(p_x)$ with only one minimum, located at

$$p_x = -\frac{\hbar m v_F e B}{p_z^2 - p_0^2}. \quad (\text{B34})$$

Expanding $V(p_x)$ around this minimum by Δp_x , the Schrodinger equation again becomes that of a harmonic oscillator:

$$(2mE)^2 \phi_2 \simeq \left[-4(\hbar m v_F e B)^2 \frac{\partial^2}{\partial p_x^2} + \dots \right. \\ \left. (p_z^2 - p_0^2)^2 + 2(p_z^2 - p_0^2) (\delta p_x)^2 \right] \phi_2. \quad (\text{B35})$$

The corresponding energy eigenvalues are

$$E = \pm \frac{1}{2m} \sqrt{(p_z^2 - p_0^2)^2 + 2\sqrt{2}\hbar m v_F e B \sqrt{p_z^2 - p_0^2} (2n+1)}. \quad (\text{B36})$$

The results from Eqs. (B33) and (B36) are plotted in Fig. 7 of the main text for $n = 0, 1, 2$.

- [1] N. Ashcroft and N. Mermin, *Solid State Physics* (Holt, Rinehart, and Winston, New York, 1976).
- [2] A. F. Ioffe, *Semiconductor Thermoelements and Thermo-Electric Cooling* (Infosearch, London, 1957).
- [3] A. Shakouri, Recent developments in semiconductor thermoelectric physics and materials, *Annu. Rev. Mater. Res.* **41**, 399 (2011).
- [4] G. J. Snyder and E. S. Toberer, Complex thermoelectric materials, *Nat. Mater.* **7**, 105 (2008).
- [5] S. M. Girvin and K. Yang, *Modern Condensed Matter Physics* (Cambridge University Press, Cambridge, 2019).
- [6] H. Fritzsche, A general expression for the thermoelectric power, *Solid State Commun.* **9**, 1813 (1971).
- [7] T. Chen and B. I. Shklovskii, Anomalously small resistivity and thermopower of strongly compensated semiconductors and topological insulators, *Phys. Rev. B* **87**, 165119 (2013).
- [8] N. P. Armitage, E. J. Mele, and A. Vishwanath, Weyl and Dirac semimetals in three-dimensional solids, *Rev. Mod. Phys.* **90**, 015001 (2018).
- [9] B. Peng, H. Zhang, H. Shao, H. Lu, D. W. Zhang, and H. Zhu, High thermoelectric performance of Weyl semimetal taas, *Nano Energy* **30**, 225 (2016).
- [10] H. Wang, X. Luo, W. Chen, N. Wang, B. Lei, F. Meng, C. Shang, L. Ma, T. Wu, X. Dai, *et al.*, Magnetic-field enhanced high-thermoelectric performance in topological Dirac semimetal Cd_3As_2 crystal, *Sci. Bull.* **63**, 411 (2018).
- [11] J. Xiang, S. Hu, M. Lyu, W. Zhu, C. Ma, Z. Chen, F. Steglich, G. Chen, and P. Sun, Large transverse thermoelectric figure of merit in a topological dirac semimetal, *Sci. China Phys. Mech. Astron.* **63**, 237011 (2019).
- [12] C. Fu, Y. Sun, and C. Felser, Topological thermoelectrics, *APL Mater.* **8**, 040913 (2020).
- [13] B. Skinner and L. Fu, Large, nonsaturating thermopower in a quantizing magnetic field, *Sci. Adv.* **4**, eaat2621 (2018).
- [14] V. Kozii, B. Skinner, and L. Fu, Thermoelectric Hall conductivity and figure of merit in Dirac/Weyl materials, *Phys. Rev. B* **99**, 155123 (2019).
- [15] E. F. Scott, K. A. Schlaak, P. Chakraborty, C. Fu, S. N. Guin, S. Khodabakhsh, A. E. Paz y Puente, C. Felser, B. Skinner, and S. J. Watzman, Doping as a tuning mechanism for magnetothermoelectric effects to improve zt in polycrystalline NbP, *Phys. Rev. B* **107**, 115108 (2023).
- [16] W. Zhang, P. Wang, B. Skinner, R. Bi, V. Kozii, C.-W. Cho, R. Zhong, J. Schneeloch, D. Yu, G. Gu, L. Fu, X. Wu, and L. Zhang, Observation of a thermoelectric Hall plateau in the extreme quantum limit, *Nat. Commun.* **11**, 1046 (2020).
- [17] F. Han, N. Andrejevic, T. Nguyen, V. Kozii, Q. T. Nguyen, T. Hogan, Z. Ding, R. Pablo-Pedro, S. Parjan, B. Skinner, A. Alatas, E. Alp, S. Chi, J. Fernandez-Baca, S. Huang, L. Fu, and M. Li, Quantized thermoelectric Hall effect induces giant power factor in a topological semimetal, *Nat. Commun.* **11**, 6167 (2020).
- [18] S. J. Watzman, T. M. McCormick, C. Shekhar, S.-C. Wu, Y. Sun, A. Prakash, C. Felser, N. Trivedi, and J. P. Heremans, Dirac dispersion generates unusually large Nernst effect in Weyl semimetals, *Phys. Rev. B* **97**, 161404 (2018).
- [19] T. Liang, J. Lin, Q. Gibson, T. Gao, M. Hirschberger, M. Liu, R. J. Cava, and N. P. Ong, Anomalous Nernst effect in the Dirac semimetal Cd_3As_2 , *Phys. Rev. Lett.* **118**, 136601 (2017).

- [20] Z. Zhu, X. Lin, J. Liu, B. Fauqué, Q. Tao, C. Yang, Y. Shi, and K. Behnia, Quantum oscillations, thermoelectric coefficients, and the Fermi surface of semimetallic WTe_2 , *Phys. Rev. Lett.* **114**, 176601 (2015).
- [21] H. Wang, X. Luo, K. Peng, Z. Sun, M. Shi, D. Ma, N. Wang, T. Wu, J. Ying, Z. Wang, and X. Chen, Magnetic field-enhanced thermoelectric performance in Dirac semimetal Cd_3As_2 crystals with different carrier concentrations, *Adv. Funct. Mater.* **29**, 1902437 (2019).
- [22] I. Obraztsov, Thermal EMF of semiconductors in a quantizing magnetic field (thermoelectromotive force of semiconductors in strong magnetic field where effect of current carrier scattering is negligible), *Fiz. Tverd. Tela* **7**, 573 (1965).
- [23] P. S. Zyryanov and G. I. Guseva, Quantum theory of thermomagnetic phenomena in metals and semiconductors, *Sov. Phys. Uspekhi* **11**, 538 (1969).
- [24] K. Tsendin and A. Efros, Theory of thermal EMF in a quantizing magnetic field in Kane model, *Sov. Phys. Solid State, USSR* **8**, 306 (1966).
- [25] J. P. Jay-Gerin, Thermoelectric power of semiconductors in the extreme quantum limit. I. The “electron-diffusion” contribution, *J. Phys. Chem. Solids* **35**, 81 (1974).
- [26] S. M. Girvin and M. Jonson, Inversion layer thermopower in high magnetic field, *J. Phys. C: Solid State Phys.* **15**, L1147 (1982).
- [27] D. L. Bergman and V. Oganessian, Theory of dissipationless Nernst effects, *Phys. Rev. Lett.* **104**, 066601 (2010).
- [28] A. A. Abrikosov, *Fundamentals of the Theory of Metals* (Courier Dover Publications, Mineola, NY, 2017).
- [29] T. Liang, Q. Gibson, J. Xiong, M. Hirschberger, S. P. Koduvayur, R. J. Cava, and N. P. Ong, Evidence for massive bulk Dirac fermions in $\text{Pb}_{1-x}\text{Sn}_x\text{Se}$ from Nernst and thermopower experiments, *Nat. Commun.* **4**, 1 (2013).
- [30] C. Fang, H. Weng, X. Dai, and Z. Fang, Topological nodal line semimetals, *Chin. Phys. B* **25**, 117106 (2016).
- [31] A. A. Burkov, M. D. Hook, and L. Balents, Topological nodal semimetals, *Phys. Rev. B* **84**, 235126 (2011).
- [32] G. Xu, H. Weng, Z. Wang, X. Dai, and Z. Fang, Chern semimetal and the quantized anomalous Hall effect in HgCr_2Se_4 , *Phys. Rev. Lett.* **107**, 186806 (2011).
- [33] Y. Chen, Y. Xie, S. A. Yang, H. Pan, F. Zhang, M. L. Cohen, and S. Zhang, Nanostructured carbon allotropes with Weyl-like loops and points, *Nano Lett.* **15**, 6974 (2015).
- [34] W. L. Min-Xue Yang and W. Chen, Quantum transport in topological nodal-line semimetals, *Adv. Phys.: X* **7**, 2065216 (2022).
- [35] X. Feng and B. Skinner, Large enhancement of thermopower at low magnetic field in compensated semimetals, *Phys. Rev. Mater.* **5**, 024202 (2021).
- [36] E. H. Hwang, E. Rossi, and S. Das Sarma, Theory of thermopower in two-dimensional graphene, *Phys. Rev. B* **80**, 235415 (2009).
- [37] L. D. Landau and E. M. Lifshitz, *Statistical Physics, Part I* (Pergamon Press, Oxford, 1980), Vol. 5.
- [38] B. I. Halperin, Quantized Hall conductance, current-carrying edge states, and the existence of extended states in a two-dimensional disordered potential, *Phys. Rev. B* **25**, 2185 (1982).
- [39] A. K. Geim and K. S. Novoselov, The rise of graphene, *Nat. Mater.* **6**, 183 (2007).
- [40] L. M. Schoop, M. N. Ali, C. Straßer, A. Topp, A. Varykhalov, D. Marchenko, V. Duppe, S. S. P. Parkin, B. V. Lotsch, and C. R. Ast, Dirac cone protected by non-symmmorphic symmetry and three-dimensional Dirac line node in ZrSiS , *Nat. Commun.* **7**, 11696 (2016).
- [41] D. Takane, Z. Wang, S. Souma, K. Nakayama, C. X. Trang, T. Sato, T. Takahashi, and Y. Ando, Dirac-node arc in the topological line-node semimetal HfSiS , *Phys. Rev. B* **94**, 121108 (2016).
- [42] L. S. Xie, L. M. Schoop, E. M. Seibel, Q. D. Gibson, W. Xie, and R. J. Cava, A new form of Ca_3P_2 with a ring of Dirac nodes, *APL Mater.* **3**, 083602 (2015).
- [43] Y. Kim, B. J. Wieder, C. L. Kane, and A. M. Rappe, Dirac line nodes in inversion-symmetric crystals, *Phys. Rev. Lett.* **115**, 036806 (2015).
- [44] Y. Huh, E.-G. Moon, and Y. B. Kim, Long-range Coulomb interaction in nodal-ring semimetals, *Phys. Rev. B* **93**, 035138 (2016).
- [45] S. V. Syzranov and B. Skinner, Electron transport in nodal-line semimetals, *Phys. Rev. B* **96**, 161105 (2017).
- [46] J.-W. Rhim and Y. B. Kim, Landau level quantization and almost flat modes in three-dimensional semimetals with nodal ring spectra, *Phys. Rev. B* **92**, 045126 (2015).
- [47] Z. Yan, R. Bi, H. Shen, L. Lu, S.-C. Zhang, and Z. Wang, Nodal-link semimetals, *Phys. Rev. B* **96**, 041103 (2017).
- [48] T. Feng, P. Wang, Z. Han, L. Zhou, W. Zhang, Q. Liu, and W. Liu, Large transverse and longitudinal magneto-thermoelectric effect in polycrystalline nodal-line semimetal Mg_3Bi_2 , *Adv. Mater.* **34**, 2200931 (2022).
- [49] R. Singha, A. K. Pariari, B. Satpati, and P. Mandal, Large nonsaturating magnetoresistance and signature of nondegenerate Dirac nodes in ZrSiS , *Proc. Natl. Acad. Sci.* **114**, 2468 (2017).
- [50] G. Hussain, X. Rao, N. Li, W. Chu, X. Liu, X. Zhao, and X. Sun, Electron transport in Dirac nodal-line semimetal ZrSiS , *Phys. Lett. A* **384**, 126938 (2020).
- [51] M. Neupane, I. Belopolski, M. M. Hosen, D. S. Sanchez, R. Sankar, M. Szlowska, S.-Y. Xu, K. Dimitri, N. Dhakal, P. Maldonado, P. M. Oppeneer, D. Kaczorowski, F. Chou, M. Z. Hasan, and T. Durakiewicz, Observation of topological nodal fermion semimetal phase in ZrSiS , *Phys. Rev. B* **93**, 201104 (2016).
- [52] M. Matusiak, J. R. Cooper, and D. Kaczorowski, Thermoelectric quantum oscillations in ZrSiS , *Nat. Commun.* **8**, 15219 (2017).
- [53] Y. Zhao, P. Cadden-Zimansky, Z. Jiang, and P. Kim, Symmetry breaking in the zero-energy Landau level in bilayer graphene, *Phys. Rev. Lett.* **104**, 066801 (2010).
- [54] F. Ghahari Kermani, Ph.D. thesis, Columbia University (2014).